# Soil moisture-evaporation coupling shifts into new gears under increasing $CO_2$

**Hsin Hsu** ( hhsu@gmu.edu )
George Mason University https://orcid.org/0000-0002-1489-6632
**Paul Dirmeyer**
Center for Ocean-Land-Atmosphere Studies, George Mason University https://orcid.org/0000-0003-3158-1752

**Article**

**Keywords:**

**Posted Date:** June 23rd, 2022

**DOI:** https://doi.org/10.21203/rs.3.rs-1713539/v1



**Version of Record:** A version of this preprint was published at Nature Communications on March 1st, 2023. See the published version at https://doi.org/10.1038/s41467-023-36794-5.

# Abstract

When soil moisture content (SM) falls within a transitional regime between dry and wet, it controls evaporation rates, affecting atmospheric heat and humidity. Accordingly, different SM regimes correspond to different gears of land-atmosphere coupling, affecting climate. Determining patterns of SM regimes and their future changes is imperative. Global distributions of shifts between SM regimes from eight climate models are examined. Under increasing $CO_2$, the range of SM extends into unprecedented coupling regimes in many locations. SM in many arid regions migrates from the transitional toward the dry regime, while an opposite migration appears in semiarid regions. Transitional regimes also emerge in currently humid areas of the tropics and high latitudes. These changes imply that a larger fraction of the world will evolve to experience more than one gear of land-atmosphere coupling, with the strongly coupled transitional regime growing the most. Furthermore, the locally predominant gear may change under global warming.


# Full Text

Soil moisture (SM) variability can control the water and heat fluxes at the land surface, affecting air temperature and humidity (Entekhabi et al. 1996; Bonan 2008b; Seneviratne et al. 2010; Santanello et al. 2018). This can establish feedbacks wherein, as the soil gets drier, the synchronous decrease in latent heat flux (LE, the energy used for evaporation) and increase in sensible heat flux (H) (Koster et al. 2004; Miralles et al. 2014) results in a warmer and drier overlying atmosphere (Schär et al. 1999; Santanello et al. 2005; Dirmeyer et al. 2012). Increasing SM can set opposite changes into motion – each chain of events ultimately alters cloud formation and precipitation (Eltahir and Bras, 1996; Findell and Eltahir 1997; Eltahir 1998; Koster et al. 2003; Yin et al. 2015; Sehler et al. 2020). Such positive local feedbacks play an important role in extreme events such as droughts, floods and heat waves (Zaitchik et al. 2006; Fischer et al. 2007; Hirschi et al. 2011; Herold et al. 2016; Miralles et al. 2014; Miralles et al. 2019). Furthermore, heterogeneous SM patterns that induce heterogeneous atmospheric heating and moistening can modulate mesoscale circulations and precipitation patterns (Ookouchi et al. 1984; Taylor and Ellis 2006; Taylor et al. 2011; Taylor et al. 2012; Froidevaux et al. 2014; Guillod et al. 2015; Hsu et al. 2016), triggering or maintaining mesoscale convective systems (MCSs; Klein and Taylor 2020; Gaal and Kinter 2021), and propagating drought events (Schumacher et al. 2022). All of these phenomena are rooted in the physical linkage between surface heat fluxes and SM, the foundation of SM-induced feedback.

SM-induced feedbacks can be strengthened or suspended in certain conditions. Such a shift in gears happens when surface fluxes disconnect from SM control under specific conditions (Budyko 1974; Koster and Milly 1997; Eagleson 1978; Santanello et al. 2007; Zeppetello et al. 2019). Such a disconnection is related to important SM thresholds (Fig.1): the wilting point (WP) and the critical soil moisture (CSM). WP is a criterion of vegetation hydraulic pressure that determines whether osmosis happens. When soils are

drier than WP, water is unable to enter plant roots and supply transpiration, the main evaporation component contributing to LE. Consequently, the sensitivity of evaporation to SM variability drops when SM<WP. This is called the dry regime. CSM is the transition separating causes of evaporation limitation: water availability versus energy availability (Seneviratne et al. 2010). When SM>CSM, increasing SM will not cause greater evaporation, and evaporation may even decline as very wet soils correspond to periods of rainfall, cloudiness and limited sunshine. In this wet regime, LE is also insensitive to SM variations. Only when SM is between WP and CSM, lying in the transitional regime, does LE reliably increase with increasing SM. The dry and transitional regimes together can be summarized as moisture-limited, while the wet regime is energy-limited.

Transitions among these three SM regimes have recently been shown to have potential influence on extremes. The 2010/11 flooding in northern Australia moistened the land surface beyond the usual moisture-limited regime and decoupled land from atmosphere (Lo et al. 2021). Reduced evaporation led to wetter land conditions that could maintain the flood. On the contrary, as SM dries, passing from the transitional regime to the dry regime, the available energy for surface heat fluxes goes mostly into H, exacerbating near-surface atmospheric heating. Consequently, air temperature becomes hypersensitive to declining SM, as has been evidenced in the United States (Benson and Dirmeyer 2021) and Europe (Dirmeyer et al. 2021).

Accordingly, SM regime transitions are good indicators of shifting gears between modes of local SM:LE coupling. Determining global patterns of existing SM regimes and their projected changes from state-of-the-art climate models can help indicate which gear of SM-induced feedback is dominant at any location, and how they may change. We examine daily data from eight climate models participating in the Coupled Model Intercomparison Project Phase 6 (CMIP6) from simulations proxying pre-industrial climate and warming climate (Method Summary).

## Pre-industrial and projected patterns of soil moisture regimes

Breakpoint analysis based on theoretical SM:LE behavior (Schwingshackl et al. 2017; Hsu and Dirmeyer 2022; see Methods) is used to find the two critical values, WP and CSM at each location, and determine which SM regimes are active there. A total of five candidates, representing different combinations of active SM regimes, are used to represent which regimes are active in each grid cell (bottom-left corner of Fig.2). We assign binary digits 0 and 1 to indicate the presence of the dry, transitional, and wet regime, in order, following the letter C for “candidate” (e.g., C010 for the transitional regime only). Fig.2 displays the spatial pattern of consensus SM regimes among the climate models and how they are projected to change under increasing $CO_2$. This is determined from the mode of the candidate selected among all climate models. The five colors correspond to each of the five candidates. Grid cells are colored according to the pre-industrial climate model consensus, and stars within grid cells indicate the projected

candidate in a warming climate. Note that the values of WP and CSM may also change, not only the distribution of SM (see Fig.S1 and Discussion).

Over the rainforests, candidates C001 and C011 dominate in the pre-industrial climate (Fig.2). Only for C011 does SM fall within the transitional regime in these locations, signifying active SM:LE coupling. This situation becomes more common under warming as C011 expands in area, particularly over the Amazon. Over semiarid regions such as the Sahel, Australia, and southern Great Plains, candidates C011 and 111 dominate during the pre-industrial period. Candidate 111 expands in a few of these regions under warming. In arid regions, SM does not always remain in the dry regime. C110 and C111 occupy the Sahara Desert, Chile, and Arabia. This could be because even sparse precipitation events moisten the land surface enough to spark significant evapotranspiration that registers in our breakpoint analysis. SM surpasses CSM in more locations as C111 emerges under warming. Overall, the global area where LE is sensitive to SM outside high latitudes (60°S-60°N) increases by 2.6% under global warming, as indicated by the summation of candidates for which the transitional regime is active, shown in the alluvial diagram in Fig.2.

## Model agreement regarding soil moisture regimes

The metric sum(δ), previously defined by Hsu and Dirmeyer (2022; See Methods), is used to quantify the disparity among climate model simulations of SM regimes for the pre-industrial climate (Fig.3) and how these disparities change under global warming. Similarly, its decomposition into sum($\delta_{dry}$), sum($\delta_{tran}$), and sum($\delta_{wet}$) in Fig.3 reflect the degree of disparity in simulating dry, transitional, and wet regimes individually.

Strong disparity in representing the SM transitional regime is found over rainforests (Fig.3e), especially over the Amazon, and this disagreement is largely reconciled in a warming world (Fig.3f). The dry regime is detected in few climate models around the edge of the Amazon (Fig.3c). The consensus is relatively good in semiarid regions compared to the rest of the world (Fig.3a). Disagreement is mainly found for dry regime detection (Fig.3c). Note that some climate models do not simulate a dry regime over the Sahara, as sum($\delta_{dry}$) is not zero (Fig.3b). Detection of the wet regime is also inconsistent across models (Fig.3g) and the consensus is even less under warming (Fig.3h).

The fractions of area with a change in any specific value of sum(δ) and their changes are displayed in the left-bottom bars of each panel. Disagreement regarding SM regimes is mainly contributed by sum($\delta_{dry}$). The overall consensus of modelled SM regimes increases under warming, due mainly to better agreement in the detection of transitional and wet regimes.

## Main migration tendency for soil moisture between regimes under global warming

A locally emergent SM regime does not necessarily indicate that SM is predominantly migrating into that specific regime (see Table.S1 for a local example). We examine the net migration of SM between regimes under global warming (see Methods). This yields 7 possible categories: no migration of SM or a migration of SM between any two of the three defined SM regimes. The results are shown in Fig.4 with symbols indicating different levels of agreement. The fraction of land area (60°S-60°N) within each category is displayed using the color matrix.

The tendency of SM to extend into the transitional regime grows in a warmer climate over some semiarid regions (see also Fig.S3). Over northwestern India, the Sahel, northern Australia, and central Asia, SM shifts from the dry regime to the transitional regime, as suggested by most climate models. On the other hand, over southern Africa, western and central Australia, migration is from the transitional regime to the dry regime, corresponding to the regions that C111 emerges under warming. Over arid regions, despite the strong disparity in detected SM regimes (Fig.3), how SM migrates between the regimes under warming is consistent among the climate models (Fig.4). In the Sahara, Chile, and Arabian Peninsula, SM lies more frequently in the dry regime, usually indicated by at least 6 of the 8 climate models. Migrations between the dry and transitional regimes accounts for 60% of global area (red+aqua categories in the color matrix of Fig.4). Robust results with at least 5 of 8 climate models agreeing with same tendency are often found over arid regions and semiarid regions. Generally, no significant migration of SM between the regimes due to warming is shown over the deep tropics (Fig.4). Sporadic responses are found over the Amazon and the maritime continent while spatial patterns are not homogeneous and are not consistent among the climate models.

# Discussion

SM regimes are a good determinant for the type of local land-atmosphere coupling, which is determined by the relationships between surface heat fluxes and SM (Fig. 1). Under global warming, SM can extend to unprecedented SM regimes in many locations (Fig. 2). There is a trend toward more gears of SM:LE coupling being experienced, and thus more shifting between gears, suggesting less stable hydroclimates. Specifically, more locations will experience the transitional regime while few locations show that a SM regime will vanish (Fig. 2). A consequence of this broadening of SM:LE candidates is that model consensus grows with increasing $CO_2$ (Fig. 3). For both the pre-industrial and the warming climate, SM spans at least two regimes over most of the world (Fig. 2). This suggests that evaluating the temporal variation of coupling is necessary when investigating topics relevant to land surface processes, especially for extreme events.

The WP and CSM are well defined by the breakpoint analysis (see Methods); however, WP and especially CSM can be sensitive to ecological and environmental factors. Therefore, values estimated here act as a

climatology of the varying breakpoints of each analyzed period. WP is mostly determined by soil and plant properties. For most climate models, plants are prescribed identically in piControl and 1pctCO2 simulations. This results in a neglectable change in WP under increasing $CO_2$ (Fig.S1b). CSM is affected not only by vegetation characteristics (Novák and Havrila 2006) but also climate conditions such as vapor pressure deficit and insolation (Haghighi et al. 2018; Feldman et al. 2019; Denissen et al. 2020). As these conditions do change in a warming climate, there can be a larger shift in CSM under increasing $CO_2$, as seen in Fig.S1c. Accordingly, an emerging SM regime under global warming is often not completely attributable to a shift in SM distribution, but shifts in WP or CSM may also contribute. For instance, a transitional regime is seen to emerge over the Amazon. In addition to a drier SM distribution (Fig.S1a), there is also a trend toward higher values for CSM (Fig.S1c), which embrace a wider range of SM in the transitional regime, bolstering its emergence.

SM migration between regimes under global warming (Fig. 4) shows a zonally consistent pattern, presumably due to changes in the large scale atmospheric circulation. SM migrates from the dry to transitional regimes over the Sahel, southern Arabian Peninsula, and Northern Australia. The increase in number of days that SM actively controls LE might strengthen the SM-induced feedbacks in these regions, which have been long-recognized as “hot spots” of land-atmosphere interactions (Koster et al. 2006; Zhang et al. 2008; Dirmeyer 2011; Diro et al. 2014; Hirschi et al. 2014; Liu et al. 2014; Lorenz et al. 2015; Hsu and Dirmeyer 2021).

SM regimes migrate from the transitional to dry regime over the Sahara, northern Arabian Peninsula, southern Africa, and western and central Australia. As a result, the arid regions spend more days in the dry SM regime, while the transitional semiarid to semi-humid regions spend more time in the transitional SM regime. Although this appears to correspond to the “wet gets wetter, dry gets dryer” paradigm (Held and Soden, 2006; Greve et al. 2014), results here do not necessarily suggest that transitional regions get wetter and arid regions get drier. As mentioned above, critical SM values can shift under a warmer climate and thus parts of the SM spectrum can slide into different regimes without a significant change in the SM distribution. How precipitation, LE, and temperature individually affect the shifting gears of SM:LE coupling needs to be disentangled.

Regimes detected over higher latitudes (above 50°) or higher altitudes could be underrepresented, especially for pre-industrial climate. Inactive SM:LE coupling is mainly attributed to snow cover that cuts off the connection between soil and atmosphere. For instance, C110 is suggested to best describe the SM distribution over eastern Siberia in some climate models (Fig.S2). This does not guarantee detection of a dry regime. The subarctic climate there leads to notable moist and warm conditions during summer, driving evaporation. Winter is the dry season from a precipitation perspective; however, regardless the dryness of SM, the snow cover stops the evaporation of soil moisture. As the number of days that land is covered by snow varies greatly among climate models, a less reliable result is possible over such areas (Fig. 3a&c&g). Nevertheless, a consistent pattern is seen under climate warming. In Fig. 2, C011 is expanding poleward over the North America and Eurasia. With more days without snow cover under

warming conditions, sensitivity of LE to SM emerges and land-atmosphere interactions could become important in regions where they currently are not (Dirmeyer et al. 2013).

Some locations experience different soil moisture regimes in different climate models within the same 50-year climate; such disparities can be large (Fig. 3). We argue that this disparity is not guaranteed to decline even if more climate models were included in this analysis. The metric sum(δ) quantifies uncertainties that can be extended to characterize the fidelity of projections of extreme events linked to SM:LE coupling, such as heatwaves, in multi-model analysis. Figure 3 can help to indicate the usefulness of multi-model projections relevant to land surface processes at any location.

Few climate models simulate a dry regime over the heatwave-active regions such as western North America (Fig. 2&Fig.S2). A similar pattern of biased SM dry regimes in historical simulations of climate models has been pointed out previously by comparison to observationally-constrained data sets using the same regime detection method (Hsu and Dirmeyer 2022)), wherein the dry regime is more commonly seen in North America, Europe, and Australia. However, here we have used pre-industrial simulations instead of historical simulations that correspond to the period of observational data sets, for reasons described in the Methods summary; the lack of SM dry regime is seen globally in all analyzed climate models (Fig. 2). As the dry regime is more prevalent in a warming climate (Fig. 3d), the lack of dry regime might be attributed to a wetter climate during pre-industrial period, rather than the problematic parameterization that prevents soil witness to fall below the WP. Moreover, different strategies of how climate models represent phenology (Song et al. 2021) can affect WP, introducing another uncertainty in the aggregated result of SM regime detection.

The global maps provided here can suggest locations worthy of a regional study of the physics of SM:LE coupling and atmospheric responses. For example, SM lingers more in the transitional regime over the Sahel in a warming climate. Does this only indicate more days with active SM:LE coupling, or will this strengthen the magnitude of SM:LE coupling and thus affects long-term temperature climatology? Over Australia, SM that shifts into the dry regime in the north and into the transitional regime in the south could lead to an opposing shift of gears in SM-induced feedbacks. Investigating further the underlying mechanisms and how they impact extremes can help us to understand land-atmosphere interactions, potentially aid prediction and mitigation, and assess climate vulnerabilities with a new perspective.

# Method Summary

Eight climate models participating in CMIP6 are used: MIROC6, AWI-ESM-1-1-LR, CMCC-ESM2, CanESM5, CNRM-CM6-1-HR, NorESM2-MM, IPSL-CM6A-LR, MRI-ESM2-0 (see Table.S2). These models are selected because they have provided daily SM and LE fields for DECK simulations (Eyring et al. 2016) for both the piControl simulation and 1pctCO2 simulation (data are available online at: https://esgf-node.llnl.gov/search/cmip6/) at the time of our analysis. Daily SM and LE fields are taken from these simulations. The ensemble member r1i1p1f1 is used from all simulations except for CNRM-CM6-1-HR, where r1i1p1f2 is used.

To provide a robust indication of the shifts in SM regimes under warming, analysis is performed for the part of 1pctCO2 runs spanning the 100th to 150th year, the time that the concentration of $CO_2$ passes from ~ 2.5 times the piControl level to 4 times, and is compared to the results from the 1st to 50th year of the piControl run. SM and LE fields from each model are regridded to a common 2˚ x 2˚ global grid; data are interpolated from the nearest grid cell. We note that daily LE fields are available from more models than daily H fields, so that SM:LE is used here to determine SM regimes. The piControl simulation is used instead of the historical simulation as the baseline for comparison because it is more consistent with 1pctCO2 runs. The historical simulation includes forcings in addition to greenhouse gases, such as land cover change and aerosol variability, that complicate diagnoses; comparison between piControl and 1pctCO2 runs yields a pure assessment of the response to increasing $CO_2$.

# Soil moisture regime determination

Segmented regression (Schwingshackl et al. 2017; Hsu and Dirmeyer 2022) is used to define the two soil moisture thresholds (WP and CSM) as breakpoints in piecewise linear fits to data where SM is the independent variable. This analysis is performed for each model and simulation. At each grid cell, five different segmented regression candidates are fitted to the distribution of available total daily LE versus SM for each simulation by each climate model; these segmented regression candidates are determined as follows: Locally, at least one SM regime (dry, transitional, or wet regime), to a maximum of the three SM regimes, can be determined depending on whether either or both of the SM thresholds are detected. This yields six possible combinations of SM regimes, called candidates: a solely dry regime, a solely transitional regime, a solely wet regime, a dry + transitional regime, a transitional + wet regime, and a dry + transitional + wet regime.

A solely dry or wet regime with SM:LE dependency is indicated by a one-segment regression with zero slope (candidates C100 or C001). These are found to arise almost exclusively over rainforests and at high latitudes where soils are almost always wet. Rare cases can also be found at coastal regions dominated by maritime air. Thus, we treat all zero-slope cases as candidate C001. A solely transitional regime is indicated by a one-segment regression consisting of a segment with positive slope (C010). Two segment regressions have one breakpoint. A dry + transitional regime is indicated by a two-segment regression consisting of a constant (dry) segment followed by a positive slope segment (C110). Transitional + wet regime is indicated by two-segment regression consisting of a positive slope segment followed by a constant (wet) segment (C011). A full dry + transitional + wet regime is indicated by the candidate with a three segmented regression and two breakpoints, consisting of a positive slope connecting two constant segments (C111).

Bayesian information criterion (BIC) for statistic model selection (Schwarz 1978) is used to select the best fit among the five segmented regression candidates:

$$BIC = n\ln(RSS/n) + k\ln(n)$$

where $n$ is the sample size, $RSS$ is the residual sum of squares, and $k$ is the number of model parameters, which is used to penalize regressions with more complex structure to prevent overfitting. At the same time, values of the WP and CSM, if detected by the best fitted regression, are recorded at each grid cell. It is possible for WP or CSM to change between simulations for the same model, and this aspect is also investigated.

# Agreement of model soil moisture regimes

We have previously designed an index δ to count the number of SM regimes for which the detection disagrees between any two candidates (Hsu and Dirmeyer 2022).

$$\delta = |a - x| + |b - y| + |c - z|$$

where *a*, *b*, and *c* are the dry, transitional and wet binary bit, respectively, of a candidate value (e.g., for a particular model); *x, y*, and *z* represent the same digits as *a*, *b*, and *c* for another source of candidate values (e.g., for validation data). For example, candidate 001 and candidate 110 have bitwise opposite detected regimes resulting in a maximal $\delta = 3$. Candidate 111 and candidate 110 only have disagreement on detection of the wet regime and thus $\delta = 1$. By replacing *x*, *y*, and *z* with the digits of the mode of the candidate obtained among all climate models, *δ* can represent how a specific climate model departs from the multi-model consensus. Accordingly, the summation of the *δ* values obtained for all pairs of each available climate model and the mode can represent how disparately the climate models simulate local SM regimes. Consequently, the lower the summation of *δ*, the better the agreement and the stronger the consensus of SM regimes among the climate models.

# Migration of soil moisture among regimes

The fraction of days that SM stays in each SM regime is calculated for each simulation. The changes of these fractions are calculated for days that SM stays in the same regime between piControl and 1pctCO2 (Fig.S3). Then, the chi-square of independence test (McHugh 2013) is applied to determine if the change of the fraction is statistically significant. If a difference in the fraction of days for any of the three regimes is significant at the 95% confidence level, the regime with the largest decrease is tagged as the regime that SM shifts out of, while the regime with the largest increase is tagged as the regime that SM shifts into. These tags yield seven categories: no statistically significant migration of SM or a migration of SM between two of the three SM regimes. Finally, the mode of the category is obtained for each grid cell from the same grid cell of each simulation by each climate model.

# Declarations


### Acknowledgements

This work was supported by National Aeronautics and Space Administration (NASA) grant 80NSSC20K1803.

### Data availability

CMIP6 model data are available at: https://esgf-node.llnl.gov/search/cmip6/. Source code of analysis and plots are available at https://github.com/hhsu81819/Soil-moisture-regime-and-projection. The alluvial diagram in Fig.2 is generated by: https://www.mathworks.com/matlabcentral/fileexchange/66746-alluvial-flow-diagram.

## References


1.

Benson, D. O. & Dirmeyer, P. A. Characterizing the Relationship between Temperature and Soil Moisture Extremes and Their Role in the Exacerbation of Heat Waves over the Contiguous United States. *Journal of Climate* **34**, 2175–2187 (2021).

2.

Bonan, G. B. Forests and Climate Change: Forcings, Feedbacks, and the Climate Benefits of Forests. *Science* **320**, 1444–1449 (2008).

3.

Denissen, J. M. C., Teuling, A. J., Reichstein, M. & Orth, R. Critical Soil Moisture Derived From Satellite Observations Over Europe. *J. Geophys. Res. Atmos.* **125**, (2020).

4.

Dirmeyer, P. A. The terrestrial segment of soil moisture-climate coupling: SOIL MOISTURE-CLIMATE COUPLING. *Geophys. Res. Lett.* **38**, n/a-n/a (2011).

5.

Dirmeyer, P. A., Balsamo, G., Blyth, E. M., Morrison, R. & Cooper, H. M. Land-Atmosphere Interactions Exacerbated the Drought and Heatwave Over Northern Europe During Summer 2018. *AGU Advances* **2**, (2021).

6.

Dirmeyer, P. A. *et al.* Evidence for Enhanced Land–Atmosphere Feedback in a Warming Climate. *Journal of Hydrometeorology* **13**, 981–995 (2012).

7.

Dirmeyer, P. A., Jin, Y., Singh, B. & Yan, X. Trends in Land–Atmosphere Interactions from CMIP5 Simulations. *Journal of Hydrometeorology* **14**, 829–849 (2013).

8.

Diro, G. T. *et al.* Land-atmosphere coupling over North America in CRCM5. *J. Geophys. Res. Atmos.* **119**, (2014).

9.

Eagleson, P. S. Climate, soil, and vegetation: 4. The expected value of annual evapotranspiration. *Water Resour. Res.* **14**, 731–739 (1978).

10.

Eltahir, E. A. B. A Soil Moisture-Rainfall Feedback Mechanism: 1. Theory and observations. *Water Resour. Res.* **34**, 765–776 (1998).

11.

Eltahir, E. A. B. & Bras, R. L. Precipitation recycling. *Rev. Geophys.* **34**, 367–378 (1996).

12.

Entekhabi, D., Rodriguez-Iturbe, I. & Castelli, F. Mutual interaction of soil moisture state and atmospheric processes. *Journal of Hydrology* **184**, 3–17 (1996).

13.

Eyring, V. *et al.* Overview of the Coupled Model Intercomparison Project Phase 6 (CMIP6) experimental design and organization. *Geosci. Model Dev.* **9**, 1937–1958 (2016).

14.

Feldman, A. F., Short Gianotti, D. J., Trigo, I. F., Salvucci, G. D. & Entekhabi, D. Satellite-Based Assessment of Land Surface Energy Partitioning–Soil Moisture Relationships and Effects of Confounding Variables. *Water Resour. Res.* **55**, 10657–10677 (2019).

15.

Findell, K. L. & Eltahir, E. A. B. An analysis of the soil moisture-rainfall feedback, based on direct observations from Illinois. *Water Resour. Res.* **33**, 725–735 (1997).

16.

Fischer, E. M., Seneviratne, S. I., Lüthi, D. & Schär, C. Contribution of land-atmosphere coupling to recent European summer heat waves. *Geophys. Res. Lett.* **34**, L06707 (2007).

17.

Froidevaux, P., Schlemmer, L., Schmidli, J., Langhans, W. & Schär, C. Influence of the Background Wind on the Local Soil Moisture–Precipitation Feedback. *Journal of the Atmospheric Sciences* **71**, 782–799 (2014).

18.

Gaal, R. & Kinter, J. L. Soil Moisture Influence on the Incidence of Summer Mesoscale Convective Systems in the U.S. Great Plains. *Monthly Weather Review* **149**, 3981–3994 (2021).

19.

Greve, P. *et al.* Global assessment of trends in wetting and drying over land. *Nature Geosci* **7**, 716–721 (2014).

20.

Guillod, B. P., Orlowsky, B., Miralles, D. G., Teuling, A. J. & Seneviratne, S. I. Reconciling spatial and temporal soil moisture effects on afternoon rainfall. *Nat Commun* **6**, 6443 (2015).

21.

Haghighi, E., Short Gianotti, D. J., Akbar, R., Salvucci, G. D. & Entekhabi, D. Soil and Atmospheric Controls on the Land Surface Energy Balance: A Generalized Framework for Distinguishing Moisture-Limited and Energy-Limited Evaporation Regimes. *Water Resour. Res.* **54**, 1831–1851 (2018).

22.

Held, I. M. & Soden, B. J. Robust Responses of the Hydrological Cycle to Global Warming. *Journal of Climate* **19**, 5686–5699 (2006).

23.

Hirschi, M., Mueller, B., Dorigo, W. & Seneviratne, S. I. Using remotely sensed soil moisture for land–atmosphere coupling diagnostics: The role of surface vs. root-zone soil moisture variability. *Remote Sensing of Environment* **154**, 246–252 (2014).

24.

Hirschi, M. *et al.* Observational evidence for soil-moisture impact on hot extremes in southeastern Europe. *Nature Geosci* **4**, 17–21 (2011).

25.

Hsu, H. & Dirmeyer, P. A. Nonlinearity and Multivariate Dependencies in the Terrestrial Leg of Land-Atmosphere Coupling. *Water Res.* **57**, (2021).

26.

Hsu, H. & Dirmeyer, P. A. Deconstructing the soil moisture-latent heat flux relationship: the range of coupling regimes experienced and the presence of nonlinearity within the sensitive regime. *Journal of Hydrometeorology* **1**, (2022).

27.

Hsu, H., Lo, M.-H., Guillod, B. P., Miralles, D. G. & Kumar, S. Relation between precipitation location and antecedent/subsequent soil moisture spatial patterns: Precipitation-Soil Moisture Coupling. *J. Geophys. Res. Atmos.* **122**, 6319–6328 (2017).

28.

Klein, C. & Taylor, C. M. Dry soils can intensify mesoscale convective systems. *Proc. Natl. Acad. Sci. U.S.A.* **117**, 21132–21137 (2020).

29.

Koster, R. D. *et al.* Regions of Strong Coupling Between Soil Moisture and Precipitation. *Science* **305**, 1138–1140 (2004).

30.

Koster, R. D. & Milly, P. C. D. The Interplay between Transpiration and Runoff Formulations in Land Surface Schemes Used with Atmospheric Models. *J. Climate* **10**, 1578–1591 (1997).

31.

Koster, R. D., Suarez, M. J., Higgins, R. W. & Van den Dool, H. M. Observational evidence that soil moisture variations affect precipitation: SOIL MOISTURE'S EFFECTS ON PRECIPITATION. *Geophys. Res. Lett.* **30**, n/a-n/a (2003).

32.

Koster, R. D. *et al.* GLACE: The Global Land–Atmosphere Coupling Experiment. Part I: Overview. *Journal of Hydrometeorology* **7**, 590–610 (2006).

33.

Liu, D., Wang, G., Mei, R., Yu, Z. & Gu, H. Diagnosing the Strength of Land–Atmosphere Coupling at Subseasonal to Seasonal Time Scales in Asia. *Journal of Hydrometeorology* **15**, 320–339 (2014).

34.

Lo, M.-H. *et al.* Temporal Changes in Land Surface Coupling Strength: An Example in a Semi-Arid Region of Australia. *Journal of Climate* **34**, 1503–1513 (2021).

35.

Lorenz, R., Pitman, A. J., Hirsch, A. L. & Srbinovsky, J. Intraseasonal versus Interannual Measures of Land–Atmosphere Coupling Strength in a Global Climate Model: GLACE-1 versus GLACE-CMIP5 Experiments in ACCESS1.3b. *Journal of Hydrometeorology* **16**, 2276–2295 (2015).

36.

Miralles, D. G., Gentine, P., Seneviratne, S. I. & Teuling, A. J. Land-atmospheric feedbacks during droughts and heatwaves: state of the science and current challenges: Land feedbacks during droughts and heatwaves. *Ann. N.Y. Acad. Sci.* **1436**, 19–35 (2019).

37.

Miralles, D. G., Teuling, A. J., van Heerwaarden, C. C. & Vilà-Guerau de Arellano, J. Mega-heatwave temperatures due to combined soil desiccation and atmospheric heat accumulation. *Nature Geosci* **7**, 345–349 (2014).

38.

Novák, V. & Havrila, J. Method to estimate the critical soil water content of limited availability for plants. *Biologia* **61**, S289–S293 (2006).

39.

Santanello, J. A. *et al.* Land–Atmosphere Interactions: The LoCo Perspective. *Bulletin of the American Meteorological Society* **99**, 1253–1272 (2018).

40.

Santanello, J. A., Friedl, M. A. & Ek, M. B. Convective Planetary Boundary Layer Interactions with the Land Surface at Diurnal Time Scales: Diagnostics and Feedbacks. *Journal of Hydrometeorology* **8**, 1082–1097 (2007).

41.

Santanello, J. A., Friedl, M. A. & Kustas, W. P. An Empirical Investigation of Convective Planetary Boundary Layer Evolution and Its Relationship with the Land Surface. *Journal of Applied Meteorology* **44**, 917–932 (2005).

42.

Schär, C., Lüthi, D., Beyerle, U. & Heise, E. The Soil–Precipitation Feedback: A Process Study with a Regional Climate Model. *J. Climate* **12**, 722–741 (1999).

43.

Schumacher, D. L., Keune, J., Dirmeyer, P. & Miralles, D. G. Drought self-propagation in drylands due to land–atmosphere feedbacks. *Nat. Geosci.* **15**, 262–268 (2022).

44.

Schwarz, G. Estimating the Dimension of a Model. *Ann. Statist.* **6**, (1978).

45.

Schwingshackl, C., Hirschi, M. & Seneviratne, S. I. Quantifying Spatiotemporal Variations of Soil Moisture Control on Surface Energy Balance and Near-Surface Air Temperature. *Journal of Climate* **30**, 7105–7124 (2017).

46.

Sehler, R., Li, J., Reager, J. & Ye, H. Investigating Relationship Between Soil Moisture and Precipitation Globally Using Remote Sensing Observations. *Journal of Contemporary Water Research & Education* **168**, 106–118 (2019).

47.

Seneviratne, S. I. *et al.* Investigating soil moisture–climate interactions in a changing climate: A review. *Earth-Science Reviews* **99**, 125–161 (2010).

48.

Song, X., Wang, D.-Y., Li, F. & Zeng, X.-D. Evaluating the performance of CMIP6 Earth system models in simulating global vegetation structure and distribution. *Advances in Climate Change Research* **12**, 584–595 (2021).

49.

Taylor, C. M., de Jeu, R. A. M., Guichard, F., Harris, P. P. & Dorigo, W. A. Afternoon rain more likely over drier soils. *Nature* **489**, 423–426 (2012).

50.

Taylor, C. M. & Ellis, R. J. Satellite detection of soil moisture impacts on convection at the mesoscale. *Geophys. Res. Lett.* **33**, L03404 (2006).

51.

Taylor, C. M. *et al.* Frequency of Sahelian storm initiation enhanced over mesoscale soil-moisture patterns. *Nature Geosci* **4**, 430–433 (2011).

52.

Taylor, C. M., Harding, R. J., Thorpe, A. J. & Bessemoulin, P. A mesoscale simulation of land surface heterogeneity from HAPEX-Sahel. *Journal of Hydrology* **188–189**, 1040–1066 (1997).

53.

Vargas Zeppetello, L. R., Battisti, D. S. & Baker, M. B. The Origin of Soil Moisture Evaporation “Regimes”. *Journal of Climate* **32**, 6939–6960 (2019).

54.

Yin, J., Albertson, J. D., Rigby, J. R. & Porporato, A. Land and atmospheric controls on initiation and intensity of moist convection: CAPE dynamics and LCL crossings. *Water Resour. Res.* **51**, 8476–8493 (2015).

55.

Zaitchik, B. F., Macalady, A. K., Bonneau, L. R. & Smith, R. B. Europe’s 2003 heat wave: a satellite view of impacts and land–atmosphere feedbacks. *Int. J. Climatol.* **26**, 743–769 (2006).

56.

Zhang, J., Wang, W.-C. & Wei, J. Assessing land-atmosphere coupling using soil moisture from the Global Land Data Assimilation System and observational precipitation. *J. Geophys. Res.* **113**, D17119 (2008).

57.

Budyko, M.I. (1974) Climate and Life. Xvii, Academic Press, New York.

# Figures

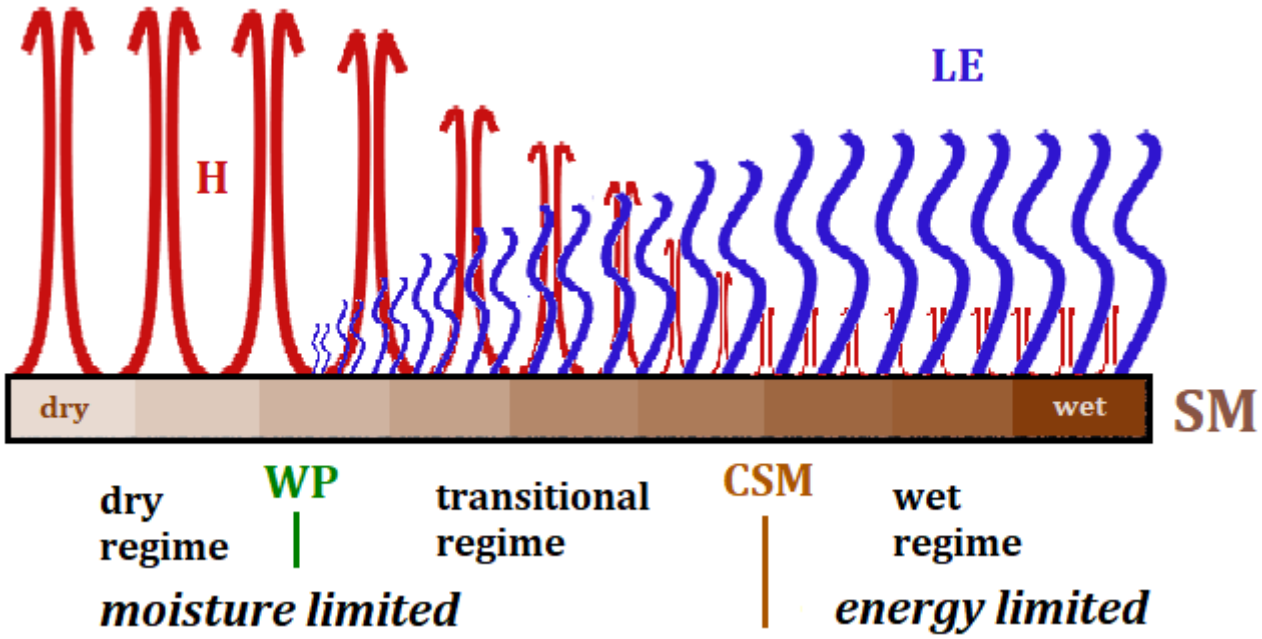


Figure 1

**The influence of soil moisture on the partitioning of surface heat fluxes with a fixed amount of available energy.**

The full range of SM can be separated into dry, transitional, and wet regimes by the thresholds of SM (wilting point WP and critical soil moisture CSM) or can be separated as moisture limited conditions and energy limited conditions separated by CSM. The transitional regime between WP and CSM is where latent heat (LE; the energy that supplies evaporation) and sensible heat (H) have strong sensitivity to SM variations. Given a fixed amount of available energy (net radiation minus ground heat flux), variations in LE and H are shown as a function of SM (increasing from left to right) by the vertical lengths of the blue (evaporative flux) and the red (thermal exchange) symbols, respectively. The shutdown of LE when SM falls into the dry regime leads to available energy exclusively supplying sensible heat. In the wet regime, LE ceases to increase with increasing SM.

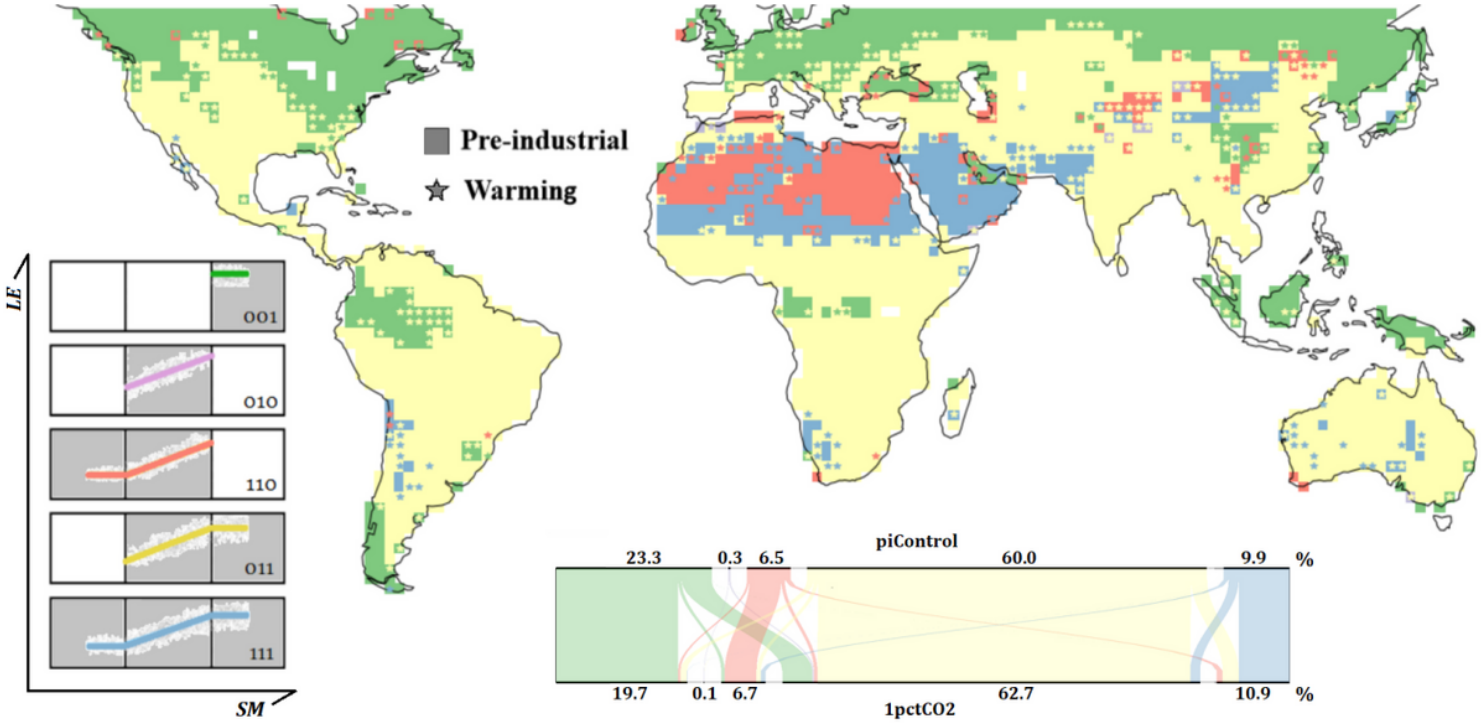


## Figure 2

**Global distribution of soil moisture regimes and their shifts under global warming.**

SM regimes at each grid cell determined by the multi-model mode of the selected segmented regression candidate among the five depicted on the left: wet regime (a.k.a. energy limited; green), transitional regime (purple), dry+transitional (a.k.a. moisture limited; orange), transitional+wet (yellow) and dry+transitional+wet (blue). For the candidate schematics on the left, soil moisture (SM) increases along the x-axis, and evaporation rate (LE) increases along the y-axis. In the global map (60°S-60°N), the color of each grid cell represents the elected candidate from the pre-industrial climate and the star color indicates a new candidate emerging in a warming climate at that grid cell. The alluvial diagram at the bottom shows the shift in the coverage of each candidate, calculated as the percentage of the global land area between 60°S to 60°N.

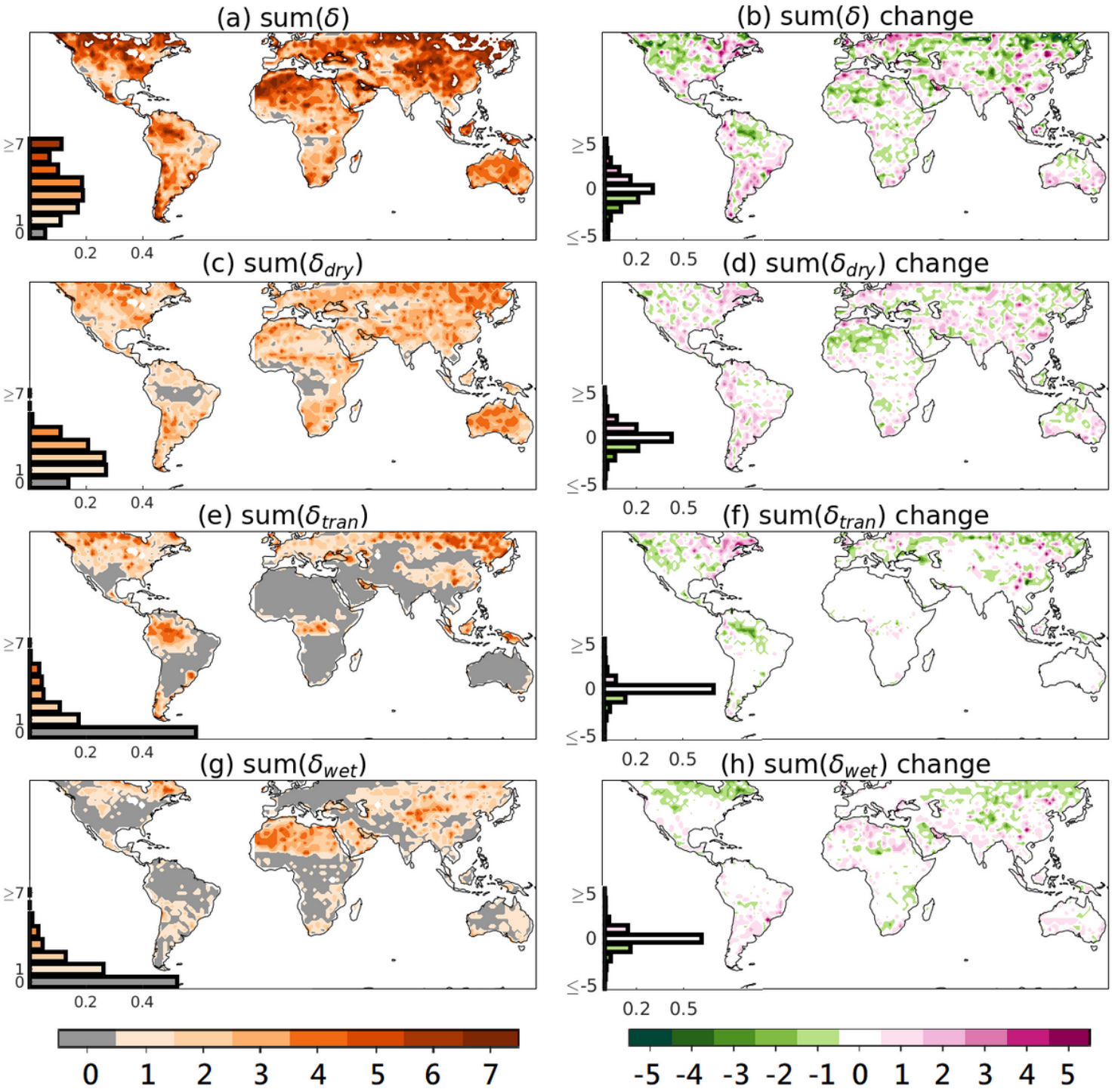


**Figure 3**

**The disparity of soil moisture regimes among climate models and their changes under global warming.**

Sum(δ) quantifies the disparity among models in SM regimes compared to the multi-model consensus (see Methods for formulation); larger sum(δ) indicates greater disparity and thus the lower consensus. Panel (a) displays sum(δ) for piControl simulations. Panel (b) displays the sum(δ) change under global warming (1pctC02 minus piControl). Panels (c), (e), and (g) display the individual consensus of detection

of the dry, transitional, and wet regimes, respectively. Panels (d), (f), and (h) display the corresponding changes in the consensus under global warming. Histograms in each panel display the fractional land area (60°S to 60°N) having the specific value of sum(δ) or change in sum(δ).

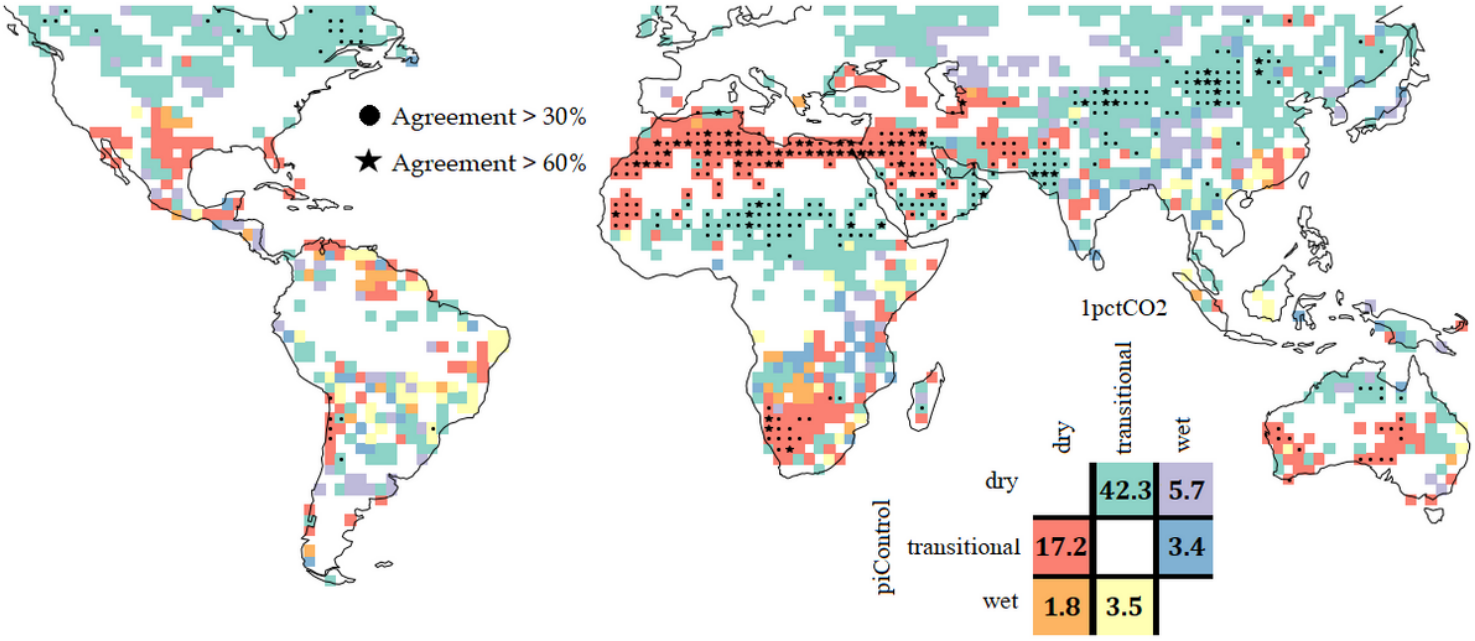


**Figure 4**

**The main migration of soil moisture frequency between regimes under global warming.**

For each climate model, the change in the percentage of days (1pctCO2 minus piControl) that SM is in each regime is calculated and its significance is tested by a chi square test of independence with $p<0.05$. If no significant difference in at least one SM regime is found, that grid cell is classified as experiencing no migration (blank). If there is a significant difference in any SM regime, a net migration is classified as a shift from the SM regime with the largest decrease in frequency to the regime that has the largest increase. The main migration is obtained by the mode among the climate models. Grid cells with agreement of at least 3 of 8 models are marked with dots; agreements of at least 5 of 8 models are marked with stars. The color key also displays the percentage of land area (60°S-60°N) experiencing each migration in a warming climate (26.1% of global land area has no migration).

# Supplementary Files

This is a list of supplementary files associated with this preprint. Click to download.

- SupInformation.docx